

Cite this: *Chem. Commun.*, 2019, 55, 482Received 3rd October 2018,  
Accepted 14th November 2018

DOI: 10.1039/c8cc07912a

rsc.li/chemcomm

## Heavy atom labeling enables silanol defect visualization in silicalite-1 crystals†

Teng Li,<sup>a</sup> Frank Krumeich,<sup>a</sup> Johannes Ihli,<sup>b</sup> Zhiqiang Ma,<sup>a</sup> Takashi Ishikawa,<sup>b</sup> Ana B. Pinar<sup>b</sup> and Jeroen A. van Bokhoven<sup>b</sup> \*<sup>ab</sup>

**Using heavy-atom labeling in conjunction with electron microscopy, we here visualize the distribution of point defects, i.e. internal silanol groups, in silicalite-1 zeolites at the single crystal level.**

Defect sites are among the dominant factors defining the activity, functionality and stability of heterogeneous catalysts.<sup>1–5</sup> Among the manifold catalysts with crystalline structures, zeolites are a fundamental pillar of the refining and petrochemical industries.<sup>6–8</sup> These microporous materials find utilization in catalysis and separation. The type and the density of structural defects strongly influence the catalytic activity.<sup>9–11</sup> For example, in the methane to hydrocarbon process, such defects can accommodate coke molecules which leads to a more pronounced deactivation of catalysts.<sup>11</sup> In addition, the distribution of structural defects is also important, since it has an impact on the structural stability. This is of particular industrial interest as simple base leaching has been shown to be an effective means to produce mesoporous or hollow zeolites.<sup>12,13</sup> Studies suggest that the dissolution and thus mesopore formation are mainly driven by inherent inhomogeneous aluminum distribution<sup>14,15</sup> and/or appearance of defect sites.<sup>16,17</sup> The formation of mesopores preferentially commences at the location of defects, as such an area is easily attacked and eliminated.

Silicate zeolites attract lots of attention due to their high thermal stability and hydrophobicity.<sup>18,19</sup> Such materials, built from corner-sharing SiO<sub>4</sub>– tetrahedra, possess two types of silanol groups, either located on the outermost surface of the crystals or within their interior in the micropores. The internal silanol groups or nests, originating due to the absence of silicon atoms in the framework, are regarded as a specific type of point defect of zeolites.<sup>20,21</sup> Unlike intergrowth and stacking

faults that have been identified by electron microscopy,<sup>22–24</sup> a direct observation of local defects with electron microscopy is rather difficult. This is due to the required spatial resolution, the low atomic number of silicon, the associated lack of image contrast, and the sensitivity of zeolite materials to the electron beam. Fourier-transform infrared (FT-IR) spectroscopy and nuclear magnetic resonance (NMR) spectroscopy are mainly used to identify the presence and the density of the silanol groups,<sup>25,26</sup> but they do not provide the needed spatial resolution to locate defects. Moreover, measuring the bulk material that has numerous crystals only gives an average result, and different crystals may possess different distributions of silanol defects. What still remains unsolved is how to visualize the location and distribution of these defects at the single crystal level. Recently, with the help of fluorescent or fluorescently labeled species, the location of real active sites was spatially identified in one zeolite crystal by fluorescence microscopy (FM).<sup>27–29</sup> The strategy of labeling may help to identify silanol defects if we can increase the contrast between the defective and the defect-free areas under electron beam conditions.

Herein, we make use of well-defined chemistry and reactivity of defect sites to visualize the distribution of silanol groups within individual crystals of silicalite-1 zeolites, and further disclose the relationship between defects and mesopore formation. This was made possible by grafting an organic moiety with an amino functional group onto the silanol defect.<sup>30,31</sup> Exposure to a suitable gold precursor resulted in heavy-atom labeled silicalite-1 with a sufficient image contrast to be observed using electron microscopy.

Fig. 1a and c show electron micrographs of the S1 (defect-rich silicalite-1) crystals which were synthesized in basic media. The crystals have a hexagonal shape of size between 200 and 300 nm. Taking advantage of hybrid pixel detectors in electron crystallography with a rotation method, our recent work shows that the S1 crystals are single crystals and not intergrown.<sup>32</sup> After mild leaching in a 0.1 M NaOH solution, mesopores were introduced (Fig. 1b and d). The preferential dissolution of the inner part was observed from both TEM and SEM. Furthermore,

<sup>a</sup> Institute for Chemical and Bioengineering, ETH Zurich, 8093 Zurich, Switzerland.  
E-mail: jeroen.vanbokhoven@chem.ethz.ch; Tel: +41 44 632 55 42

<sup>b</sup> Paul Scherrer Institute, 5232 Villigen, Switzerland

† Electronic supplementary information (ESI) available: Experimental details, characterization data and calculation methods are provided in section 1; complementary XRD, FT-IR, NMR, and TEM images are available in section 2. See DOI: 10.1039/c8cc07912a



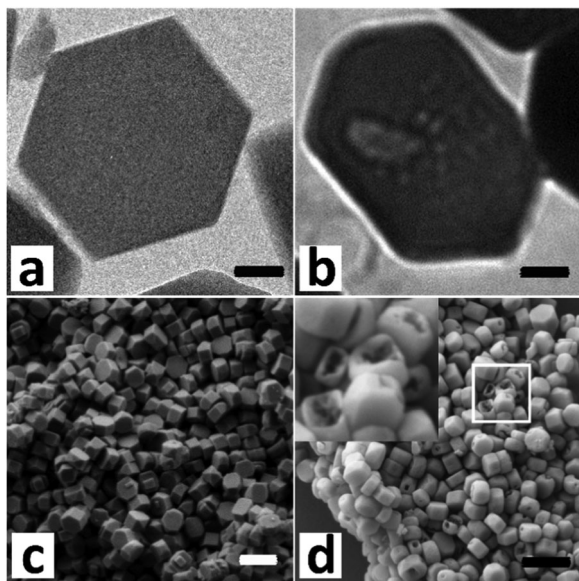
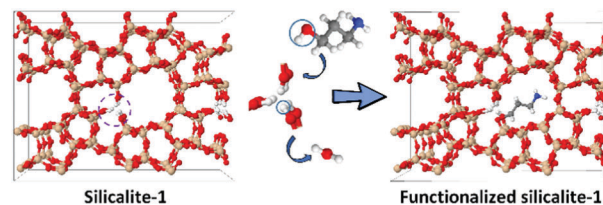


**Fig. 1** TEM and SEM images of (a and c) the defect-rich silicalite-1 and (b and d) the corresponding crystals leached in 0.1 M NaOH for 10 h. Scale bars represent 50 nm (a and b) and 500 nm (c and d). The TEM image in (b) was recorded in strong underfocus to enhance the pore visibility.

base leaching under more severe conditions leads to the formation of a hollow-like structure, manifesting a higher stability of the rim of crystals (Fig. S1, ESI†).<sup>33</sup> The crystallinity increased by 20% after mild leaching (Fig. S2a, ESI†). Regarding the -OH groups, three main peaks were observed from the infrared spectrum (Fig. S2b, ESI†), *i.e.*, which can be ascribed to the external silanols, the internal silanols and the silanol nests.<sup>34</sup> The presence of silanol nests and the high intensity ratio between  $3726\text{ cm}^{-1}$  and  $3745\text{ cm}^{-1}$  ( $I_{3726}/I_{3745} \approx 8.7$ ) implied the existence of a significant number of defects. The mild leaching eliminated most defects as the peak intensity at  $3726\text{ cm}^{-1}$  and  $3500\text{ cm}^{-1}$  decreased significantly. The  $^{29}\text{Si}$  MAS NMR result also confirmed the diminution of silanol groups. The  $\text{Q}^3$  (HO-Si-[(OSi)<sub>3</sub>]) group decreased much upon leaching (Fig. S2c, ESI†).

Organic functionalization of ordered mesoporous materials has seen significant progress.<sup>35–39</sup> Studies have proved that coupling agents of large molecular size can be more efficiently grafted than their smaller counterparts.<sup>40–42</sup> However, their grafting onto the internal surface of zeolites is inhibited by the limited micropore size. To functionalize the internal surface of silicalite-1 crystals efficiently, the size of the coupling molecule should be tuned to fit zeolite micropores. 3-Amino-1-propanol is selected here due to its linear structure and reactivity to silanol groups (Scheme 1).<sup>31</sup> The -OH group condenses with the silanol group to form a C-O-Si linkage, fixing the molecule onto the defect site. The amino group is subsequently used to anchor heavy atoms as labels. Gold is selected as the marker due to its strong interaction with the amino groups.<sup>43,44</sup>

The main grafting work strictly followed a published paper.<sup>31</sup> The weight loading of the organic moiety was measured by thermal gravimetric analysis (TGA) (Fig. S3a, ESI†). For S1, the weight loss before  $150\text{ }^\circ\text{C}$  ( $\approx 1\text{ wt}\%$ ) can be assigned to the



**Scheme 1** An illustration of the functionalization process of silicalite-1. The silanol groups react with 3-amino-1-propanol, forming a covalent bond and realizing the introduction of amino groups for subsequently anchoring gold atoms. Color scheme: brown (Si), red (O), white (H), blue (N) and gray (C).

removal of water, whereas, the decrease after  $550\text{ }^\circ\text{C}$  was caused by the condensation of neighboring silanol groups to form Si-O-Si linkages.<sup>45,46</sup> A significant weight loss (4.7 wt%) was observed for the functionalized S1 between  $250$  and  $550\text{ }^\circ\text{C}$ , caused by the removal of the organic moiety. The total organic loading is nearly  $0.82\text{ mmol g}^{-1}$ . The external surface grafting is inevitable but that part can be estimated to be as much as  $0.11\text{ mmol g}^{-1}$  (see the ESI†). The  $^{29}\text{Si}$  MAS NMR spectrum shows a significant reduction of the  $\text{Q}^3$  groups after grafting (Fig. S3b, ESI†). This is more obvious from the  $^{29}\text{Si}$  CP MAS NMR spectrum since the signals of silicon nuclei bonded to OH groups can be enhanced by the protons in proximity.<sup>17</sup> The  $\text{Q}^3/\text{Q}^4$  ratio decreased from 3.55 to 0.33 after grafting and the  $\text{Q}^2$  groups in S1 were eliminated completely (Fig. S3c, ESI†).

To introduce gold, the functionalized S1 was mixed with an aqueous solution of  $\text{HAuCl}_4$  at a pH of 2.5 ( $10^{-3}\text{ mol L}^{-1}$ ). Then, the solid was washed thoroughly and dried at room temperature. The defect-labeled S1 presents a light yellow color. The gold loading determined by atomic absorption spectroscopy (AAS) was 0.7 wt%, nearly  $0.036\text{ mmol g}^{-1}$ , much lower than the amount of the organic moiety. This indicated that not all labeled silanols were accessible by gold. One reason could be the blocking of the accessibility of the gold precursor species to the more interior part by the organic moieties that are located on or close to the external surface. The significant decrease in the micropore volume ( $\sim 45\%$ ) and the external surface area ( $\sim 80\%$ ) confirmed the existence of diffusion limitation for the functionalized S-1 (Table S1, ESI†). Adding the gold precursor into pristine S1 did not show the presence of any gold in the material, which suggested that the introduced amino groups did play a role in the attraction of gold atoms. Fig. 2a and b present the electron micrographs of the defect-labeled S1. Overall, the original shape of the crystals was preserved. A closer look at the individual crystals shows small white spots with a size between 0.8 and 1 nm (Fig. 2c–f), which were gold clusters (Z-contrast). The small sizes of gold clusters were also confirmed by XRD with no gold peak visible (Fig. S5, ESI†). Well-resolved diffraction peaks also indicated that the introduction of amino groups and gold clusters did not create new and obvious defects. The size of the clusters was larger than the pore diameter (0.55 nm), but close to the size of the channel intersection (1 nm).<sup>47</sup> Interestingly, the gold clusters were more heterogeneously distributed. Their concentration was high in



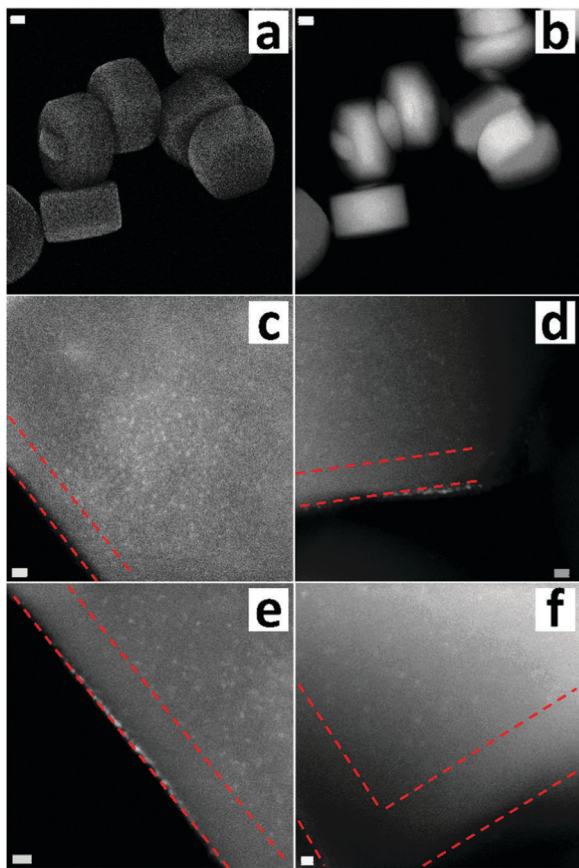


Fig. 2 (a) Secondary electron STEM and (b-f) HAADF-STEM images of defect-labeled S1. Scale bars represent 50 nm (a and b), 5 nm (c–e) and 2 nm (f). The red dashed line indicates a defect-starved rim with about 10 nm thickness.

the crystal core and on the outermost layer, whereas fewer gold clusters were detected within a 10 nanometer rim measured from the surface of the crystal. It indicated that the 10-nanometer-area from the edge possesses fewer defects than the core part. To further decrease the size of gold clusters or obtain gold single atoms, we also applied another more dilute gold solution ( $10^{-4}$  mol L $^{-1}$ ). However, after careful examination we were not able to find any trace of gold though elemental analysis indicated its existence (Fig. S6, ESI $^{\dagger}$ ). The reason was possibly the presence of the atomically dispersed gold within a thick crystal, which did not provide enough contrast for visualization. The formation of clusters was due to the aurophilicity of gold, *i.e.* the tendency to form Au–Au bonds.<sup>48</sup> This should happen on the defect site or at least close to the defective area as amino groups provided the anchoring site for landing initial gold atoms. The uneven spatial distribution of defects may be related to the crystallization process, as a slower growth rate at the later stage can lead to a better crystallized structure with fewer silicon vacancies and therefore a lower concentration of silanol defects.<sup>49,50</sup>

The defect-poor silicalite-1 sample with monoclinic symmetry (S2) was also prepared and investigated here. The pristine sample had two size populations, one with crystals between 150 and 250 nm and the other one with particles between

20 and 30 nm. The small particles may be metastable silica nanoparticle precursors since most were attached on the big ones (Fig. S7, ESI $^{\dagger}$ ).<sup>51</sup> Leaching in the 0.1 M NaOH solution eliminated most of the small particles, and a harsher treatment in the 0.2 M NaOH solution gave rise to the formation of mesopores in the big crystals. Unlike the leached S1 crystals, the mesopores were randomly distributed in the leached S2 crystals, suggesting that S2 did not have a preferential location of the defects. The intensity of the external silanols was much higher than that of the internal silanols (Fig. S8b, ESI $^{\dagger}$ ). The Q<sup>3</sup> signal was not observed in the <sup>29</sup>Si MAS NMR spectrum (Fig. S8c, ESI $^{\dagger}$ ). Such a relatively defect-poor framework structure was further confirmed as its NMR signals can be attributed to 24 inequivalent T sites within the monoclinic symmetry (Fig. S8d and Table S2, ESI $^{\dagger}$ ).<sup>52</sup> The labeling of the defects for S2 was carried out following the above described method. The lower gold loading (0.29 wt%) confirmed a low concentration of silanol groups. Fig. 3 shows the distribution of gold clusters, and the typical size of the clusters was between 1.0 and 1.5 nm, larger than that in the previous case. Such clusters were mainly located on the outermost layer of crystals. This distribution is expected since S2 has more external silanols and fewer inner defects.

The inhomogeneous aluminum distribution, such as Al-zoning, can be probed by electron microscopy and associated energy-dispersive X-ray (EDX) spectroscopy.<sup>15,53</sup> However, any distribution of point defects in zeolites has been so far only postulated. Creating a new method to visualize the distribution of such defects is necessary, since this enables getting a more direct insight into defect chemistry. Regarding the defect-rich silicalite-1, *i.e.* S1, a defect-starved rim with about 10 nm thickness was identified. As a result, the rim part was robust while more pores formed in the core during base leaching. Such a consistency was further confirmed for the defect-poor sample (S2) since it showed a much lower concentration and a random distribution of markers, and consequently a non-preferential mesopore formation.

In summary, we present a new labeling method to make the point defects visible in silicalite-1 at the single crystal level. The feasibility of the procedure is confirmed by base leaching experiments and related characterization. However, there is still a lot of space to improve this work in future studies. For example, labelling all silanols as well as visualizing atomically dispersed gold within a thick crystal will be very challenging.

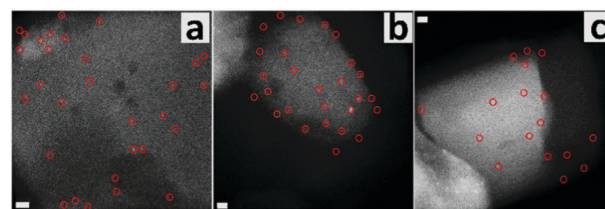


Fig. 3 STEM images of the defect-labeled S2. Scale bars are 10 nm (a) and 5 nm (b and c). Typical gold clusters on the same one crystal are indicated by red circles.



The authors thank the Scientific Center for Optical and Electron Microscopy of the ETH Zurich for technical support. The help of Mr X. Wang is acknowledged. Mr T. Li acknowledges the financial support provided by the China Scholarship Council (CSC). Dr A. B. Pinar acknowledges the Energy System Integration (ESI) platform at the Paul Scherrer Institute (PSI) for funding.

## Conflicts of interest

The authors declare no conflict of interest.

## Notes and references

- M. E. Hagerman and K. R. Poeppelmeier, *Chem. Mater.*, 1995, **7**, 602–621.
- T. Zambelli, J. Wintterlin, J. Trost and G. Ertl, *Science*, 1996, **273**, 1688–1690.
- A. M. Stoneham, *Theory of defects in solids: electronic structure of defects in insulators and semiconductors*, Oxford University Press, 2001.
- Y. Meng, W. Song, H. Huang, Z. Ren, S.-Y. Chen and S. L. Suib, *J. Am. Chem. Soc.*, 2014, **136**, 11452–11464.
- C.-Y. Wu, W. J. Wolf, Y. Levartovsky, H. A. Bechtel, M. C. Martin, F. D. Toste and E. Gross, *Nature*, 2017, **541**, 511.
- A. Corma and A. Martinez, *Adv. Mater.*, 1995, **7**, 137–144.
- J. Shi, Y. Wang, W. Yang, Y. Tang and Z. Xie, *Chem. Soc. Rev.*, 2015, **44**, 8877–8903.
- B. M. Weckhuysen and J. Yu, *Chem. Soc. Rev.*, 2015, **44**, 7022–7024.
- G. Heitmann, G. Dahlhoff and W. Hölderich, *J. Catal.*, 1999, **186**, 12–19.
- I. Yarulina, J. Goetze, C. Gücüyener, L. van Thiel, A. Dikhtiarenko, J. Ruiz-Martinez, B. M. Weckhuysen, J. Gascon and F. Kapteijn, *Catal. Sci. Technol.*, 2016, **6**, 2663–2678.
- K. Barbera, F. Bonino, S. Bordiga, T. V. Janssens and P. Beato, *J. Catal.*, 2011, **280**, 196–205.
- J. C. Groen, J. A. Moulijn and J. Pérez-Ramírez, *J. Mater. Chem.*, 2006, **16**, 2121–2131.
- L. Sommer, D. Mores, S. Svelle, M. Stöcker, B. M. Weckhuysen and U. Olsbye, *Microporous Mesoporous Mater.*, 2010, **132**, 384–394.
- C. Mei, Z. Liu, P. Wen, Z. Xie, W. Hua and Z. Gao, *J. Mater. Chem.*, 2008, **18**, 3496–3500.
- N. Danilina, F. Krumeich, S. A. Castelanelli and J. A. van Bokhoven, *J. Phys. Chem. C*, 2010, **114**, 6640–6645.
- S. Svelle, L. Sommer, K. Barbera, P. N. Vennestrom, U. Olsbye, K. P. Lillerud, S. Bordiga, Y.-H. Pan and P. Beato, *Catal. Today*, 2011, **168**, 38–47.
- D. Fodor, A. Belouqui Redondo, F. Krumeich and J. A. van Bokhoven, *J. Phys. Chem. C*, 2015, **119**, 5447–5453.
- A. Persson, B. Schoeman, J. Sterte and J.-E. Otterstedt, *Zeolites*, 1994, **14**, 557–567.
- M. A. Camblor, A. Corma and S. Valencia, *Chem. Commun.*, 1996, 2365–2366.
- M. Hunger, J. Kärger, H. Pfeifer, J. Caro, B. Zibrowius, M. Bülow and R. Mostowicz, *J. Chem. Soc., Faraday Trans. 1*, 1987, **83**, 3459–3468.
- D. F. Shantz, J. Schmedt auf der Günne, H. Koller and R. F. Lobo, *J. Am. Chem. Soc.*, 2000, **122**, 6659–6663.
- M. W. Anderson, K. S. Pachis, F. Prébin, S. W. Carr, O. Terasaki, T. Ohsuna and V. Alfreddson, *J. Chem. Soc., Chem. Commun.*, 1991, 1660–1664.
- M. Pan, *Micron*, 1996, **27**, 219–238.
- P. A. Wright, W. Zhou, J. Pérez-Pariente and M. Arranz, *J. Am. Chem. Soc.*, 2005, **127**, 494–495.
- T. Karbowski, M.-A. Saada, S. Rigolet, A. Ballandras, G. Weber, I. Bezverkhyy, M. Soulard, J. Patarin and J.-P. Bellat, *Phys. Chem. Chem. Phys.*, 2010, **12**, 11454–11466.
- E. E. Mallon, M. Y. Jeon, M. Navarro, A. Bhan and M. Tsapatsis, *Langmuir*, 2013, **29**, 6546–6555.
- M. B. Roeffaers, B. F. Sels, H. Uji-i, F. C. De Schryver, P. A. Jacobs, D. E. De Vos and J. Hofkens, *Nature*, 2006, **439**, 572.
- E. Stavitski, M. H. Kox and B. M. Weckhuysen, *Chem. – Eur. J.*, 2007, **13**, 7057–7065.
- W. Xu, J. S. Kong, Y.-T. E. Yeh and P. Chen, *Nat. Mater.*, 2008, **7**, 992.
- C.-H. Cheng, T.-H. Bae, B. A. McCool, R. R. Chance, S. Nair and C. W. Jones, *J. Phys. Chem. C*, 2008, **112**, 3543–3551.
- M. H. Kassaei, D. S. Sholl and S. Nair, *J. Phys. Chem. C*, 2011, **115**, 19640–19646.
- T. Gruene, T. Li, E. Van Genderen, A. B. Pinar and J. A. Van Bokhoven, *Chem. – Eur. J.*, 2018, **24**, 2384–2388.
- T. Li, Z. Ma, F. Krumeich, A. J. Knorpp, A. B. Pinar and J. A. Van Bokhoven, *ChemNanoMat*, 2018, **4**, 992–999.
- S. Bordiga, P. Ugliengo, A. Damin, C. Lamberti, G. Spoto, A. Zecchina, G. Spano, R. Buzzoni, L. Dalloro and F. Rivetti, *Top. Catal.*, 2001, **15**, 43–52.
- J. Beck, J. Vartuli, W. J. Roth, M. Leonowicz, C. Kresge, K. Schmitt, C. Chu, D. H. Olson, E. Sheppard and S. McCullen, *J. Am. Chem. Soc.*, 1992, **114**, 10834–10843.
- D. Zhao, Q. Huo, J. Feng, B. F. Chmelka and G. D. Stucky, *J. Am. Chem. Soc.*, 1998, **120**, 6024–6036.
- A. Vinu, K. Z. Hossain and K. Ariga, *J. Nanosci. Nanotechnol.*, 2005, **5**, 347–371.
- X. Feng, G. Fryxell, L.-Q. Wang, A. Y. Kim, J. Liu and K. Kemner, *Science*, 1997, **276**, 923–926.
- A. Benhamou, M. Baudu, Z. Derriche and J.-P. Basly, *J. Hazard. Mater.*, 2009, **171**, 1001–1008.
- E. P. Plueddemann, *Silane coupling agents*, Springer, 1991, pp. 31–54.
- T. Kawai and K. Tsutsumi, *Colloid Polym. Sci.*, 1998, **276**, 992–998.
- L. Zhang, C. Yu, W. Zhao, Z. Hua, H. Chen, L. Li and J. Shi, *J. Non-Cryst. Solids*, 2007, **353**, 4055–4061.
- P. Santhosh, A. Gopalan and K.-P. Lee, *J. Catal.*, 2006, **238**, 177–185.
- Y. K. Hwang, D. Y. Hong, J. S. Chang, S. H. Jhung, Y. K. Seo, J. Kim, A. Vimont, M. Daturi, C. Serre and G. Férey, *Angew. Chem., Int. Ed.*, 2008, **47**, 4144–4148.
- T. Masuda, S.-h. Otani, T. Tsuji, M. Kitamura and S. R. Mukai, *Sep. Purif. Technol.*, 2003, **32**, 181–189.
- J. Kuhn, S. Sutanto, J. Gascon, J. Gross and F. Kapteijn, *J. Membr. Sci.*, 2009, **339**, 261–274.
- T. Yokoi, H. Mochizuki, S. Namba, J. N. Kondo and T. Tatsumi, *J. Phys. Chem. C*, 2015, **119**, 15303–15315.
- M. Aslam, L. Fu, M. Su, K. Vijayamohan and V. P. Dravid, *J. Mater. Chem.*, 2004, **14**, 1795–1797.
- V. Nikolakis, D. G. Vlachos and M. Tsapatsis, *J. Chem. Phys.*, 1999, **111**, 2143–2150.
- C. S. Cundy and P. A. Cox, *Microporous Mesoporous Mater.*, 2005, **82**, 1–78.
- A. I. Lupulescu and J. D. Rimer, *Science*, 2014, **344**, 729–732.
- G. Engelhardt and H. Van Koningsveld, *Zeolites*, 1990, **10**, 650–656.
- J. C. Groen, T. Bach, U. Ziese, A. M. Paulaime-vanDonk, K. P. de Jong, J. A. Moulijn and J. Pérez-Ramírez, *J. Am. Chem. Soc.*, 2005, **127**, 10792–10793.

